Laser Ranging to Space Debris in Poland: Tracking and Orbit Determination

Paweł Lejba, Tomasz Suchodolski, Piotr Michałek

Centrum Badań Kosmicznych Polskiej Akademii Nauk (CBK PAN)
Borowiec Astrogeodynamic Observatory

ABSTRACT

After big modernization in 2014, the LASBOR station (CBK PAN Borowiec) has entered a new chapter of the laser measurements. With two independent Nd:YAG pulse laser modules, i.e. the standard unit used for laser observations of all satellites equipped with retroreflectors (picosecond module EKSPLA PL - 2250) and a high - energy module (nanosecond Continuum Surelite III) dedicated to Space Surveillance and Tracking (SST) activity, the station is able to track satellites (LEO and MEO), as well as space debris targets (LEO defunct satellites and rocket bodies). The tracking of typical rocket bodies has been launched in the middle of 2016. Today, the LASBOR station tracks over 100 different satellites (active / inactive) and rocket bodies. The rocket bodies are tracked for the needs of Space Surveillance and Tracking (SST) programme. During last 3.5 years (2016 - 2019), the LASBOR station performed 1123 successful passes of space debris objects, providing 13688 of normal points. An average RMS of these passes is on the level of 2 centimetres - 2 metres (depending on the laser module being used). Additionally, the LASBOR team calculated the orbits of several rocket bodies based on an one single laser track (in full rate measurements format), showing, that their covariance matrix can be improved approximately by 20 - 40 percent, even if the track has a time length of several dozen seconds. All orbital computations were performed by means of NASA Goddard's GEODYN-II program in an Earth-Centered Inertial True of Date reference frame. The input orbital elements of the targets were TLE files downloaded from the SPACETRACK database.
At Borowiec, a second independent laser - optical system is developed. This system is fully dedicated to the SST activity. The new system is situated on an azimuth / elevation mount with a 65 centimetres Cassegrain telescope equipped with servo drives that provide a tracking resolution below 1 arcsecond, and the 8 inches RC guiding telescope equipped with two fast dedicated optical CMOS cameras. The whole system is controlled by a multiplatform steering / tracking software and support space debris / satellite predictions, system calibration, ADSB monitoring, data post - processing and other functions. The new sensor will be equipped with high - powerful laser module. The objective of this action is the tracking of uncooperative LEO targets with a diameter below 1 metre and participation in the building of the independent laser catalogue in a near future. Finally, the second sensor will operate 24 hours a day, 7 days a week. At present, this system is fully operational in optical mode.

1 INTRODUCTION

Since over 15 years, the laser stations actively and promising support tracking of space debris, continuously developing and expanding capabilities of the laser sensors [1, 2, 3, 4, 5, 6, 7]. The LASBOR station also belongs to this group. The first polish Satellite Laser Ranging System was built at the beginning of 1980's by the Space Research Centre of the Polish Academy of Sciences (CBK PAN) and finally started to work in 1986. On the 13th of May 1988 CBK PAN joined to International Laser Ranging Service (ILRS) as a Borowiec laser station (LASBOR) with CDDIS SOD number 78113802 [8]. Since that time polish station has tracked many different satellites from LEO and MEO regimes. At the end of 2014 the LASBOR station was involved in Space Debris Study Group (SDSG) associating representatives of various laser centres all over the world operating at ILRS. In the middle of 2016 [9], CBK PAN has launched regular tracking of space debris targets (cooperative and uncooperative targets) from LEO regime, including inactive satellites and rocket bodies. Station was validated by ESA's space debris laser campaign in 2017 in the frame of ESA's SSA Programme [10].
Parallel to the activity mentioned above, the laser team from CBK PAN have started to develop the second independent laser - optical system fully dedicated to Space Surveillance and Tracking (SST) programme. Both laser sensors are located in western Poland and are owned by CBK PAN, branch in Borowiec Astrogeodynamic Observatory, Poland. In Figure 1 the location of the polish laser sensors is marked.

Fig.1. Location of the CBK PAN laser sensors (source: https://earth.google.com/).

Currently, the tasks related to the laser and optical measurements to space debris are continued and developed. Additionally, the LASBOR team focus on orbit determination of space debris based on laser measurements. To this work the advanced orbital programme made by NASA is used, called GEODYN-II [11]. The single passes of the tracked objects are analysed. Basing on their full rate data (single laser measurements), their orbits are calculated in order to improve their covariances. In this paper the orbital results obtained for 13 rocket bodies are presented.

2 LASER SENSOR NR 1

The mount of the laser sensor nr 1 is the azimuth / elevation type with separate optics of the transmitting and receiving systems and a guide telescope (Fig. 2). The basic parameters of the mount are shown in Table 1.


Fig. 2. Cassegrain A – laser system nr1.

Tab. 1. The main parameters of the mount nr1.

MOUNT	Az-El
Tracking	step by step
Encoder resolution	1.8 arcsec
RECEIVER	Cassegrain system
Diameter of the main mirror	65cm
Effective diameter of the main mirror	60cm
Diameter of the secondary mirror	20cm
FOV	5 arcmin
GUIDE TELESCOPE	Maksutov system
Tracking	Visual (CCD camera)
Diameter of the mirror	20cm
FOV	1^0

The motion of the mount is driven by two DC motors, which works in a step by step mode fully controlled by the computer in the range from 0.0005 to 540 degrees. The maximum revolution in azimuth amounts to 540 degrees and in elevation to 190 degrees. The maximum speed of the mount is 7 deg / sec in both axes. The time base for the system nr 1 is an active hydrogen maser CH1-75A providing 10 MHz and 1 pps time signal for laser sensor clock. The whole system is controlled by one operator. The steering / control software were made by laser team and comprises: satellite predictions preparation, real - time processing (satellite tracking), data handling and post - processing analysis. In the year 2014 the laser system nr 1 in Borowiec was modernized. A new optics was replaced in the transmitting - receiving telescope, including primary and secondary mirrors of the telescope and special dielectric mirrors transferring laser pulse from laser unit to the telescope. The second step of modernization concerned lasers. Two Nd:YAG laser modules were installed, the standard unit used for laser observations of all ILRS satellites (EKSPLA PL - 2250) and high - energy module (Continuum Surelite III) dedicated to laser observations of space debris. The second one works with 10 times stronger pulse energy than EKSPLA module. In Table 1 the main parameters of the laser modules were presented.

Tab. 2. The main parameters of the LASBOR lasers.

Parameter	EKSPLA PL-2250	Continuum Surelite III
Stand	Optical table	Optical table
Repetition rate	10 Hz	10 Hz
Pulse energy (532 nm)	0.05 J	0.45 J
Pulse length	60 ps	3-5 ns
Average power	0.5 W	4.5 W

3 LASER-OPTICAL SENSOR NR 2

The new system proposed by CBK PAN will combining laser ranging, light curves and spectography techniques (Fig. 3). The solution is based on the Az / El mount with the Cassegrain telescope with a 65 cm primary mirror and the RC8" as auxiliary telescope. The mount of the telescope in the Az / El configuration is driven by two servo drives. The drive torque is transmitted by means of multiplate couplings to the exact self-adjusting worm gears of each Az / El axis. The resulting value of the positioning system resolution is < 1 arcsec (positioning accuracy << 1 arcmin – positioning window). The drive system is powered by dedicated NC units (for each axis) supported by PLC controllers (e.g. positioning and terminal sensors). Due to the need to quickly control the system (20 Hz control loop), it was decided to use the CANBUS standard whose commands are asked from the dedicated Linux semiRT system. Installation works simultaneously in three frames of reference: the machine one (hardware), terrestial and celestial coordinates system (software computation).

Fig. 3. Cassegrain-B – laser-optical system nr2.

All automation components such as roof control, station safety systems and laser shutter are controlled by the PLC module. Electronic components (e.g. cameras) are connected by a USB3 hub placed on the telescope. At the Cassegrain telescope backfocus, a box with an optical plate was installed, which was equipped with a set of bending and dichroic mirrors. Such a system will enable the acquisition of photos with a dedicated large chip camera, acquisition of light curves and detection of 532 / 1064 nm laser photons. At the main focal point of the telescope a corrective lens with a diaphragm was mounted. The auxiliary telescope RC8" was equipped with a electronic filter changer with diffraction grating and ZWO ASI1600MMC camera (also ZWO ASI174MMC; both for tests). All components are connected by a powered USB3 hub placed on the telescope. For the needs of the tracking, a ground station was equipped with a meteo station, ADSB passive radar (with 400 km range), 70 cm RF receiver, GPS receiver (as a backup) and all-sky camera. All subsystems were developed by CBK PAN.

For the purpose of the telescope's developed control, complete software tool environment was implemented to manage the entire station (c#, mysql), operating on the linux64 semiRT platform (Fig. 4). The control room is synchronized directly with the atomic time laboratory (10 MHz and 1 pps signals) and GPS as the backup time base. The software enables a complete process of tracking an orbital object along with signal acquisition (laser, optical) and auxiliary data (weather data, aircraft radar, meteorological balloon radar). The program window contains tabs (real / simulation time visualization, objects catalogue, data update, settings, scheduling, manual movement control, current closeups, telescope service) which guide through the process of tracking.

The bottom part table and the 2D map show selected satellites for tracking (just-in-time/without planning observation task) and a list of satellites considered (right window). The program's engine is based on the SGP4 algorithm, which generates successive iterations of tracing at intervals of 50 ms in the continuous mode. It should be noted that no offline data are generated. The position parameters sent to the telescope are generated in semiRT. Time / position correction related to the delay of the algorithm's operation and related to the delay of exchanging data between PC and servo drives is determined automatically during the next (50 ms) iteration of the program's operation. The program window also contains a radar view, which shows the current satellites within the range of the station. The station system has been equipped with additional components necessary to conduct safe laser observations, which include aircraft traffic (ADSB), meteorological balloons passes (the program allows tracking balloons based on data packets transmitted in the band of 70 cm). All hardware components were made by CBK PAN Borowiec.

The control (permission) of the work of the laser beam is carried out by analysing the current air traffic (15 deg safety zone between aircraft and tracked trajectory). A relational database model was adopted in a business approach. Stored ephemeris of the satellites can be supplemented with additional data, such as: physical parameters of the satellite, radar cross-section value. The database of objects (mysql) contains all historical ephemeris of objects included in categories. Based on information about a given object, a simple analysis of orbital data can be carried out (inclination, reactance, apogee / perigee). The objects database (mysql) contains all historical ephemeris of objects. The software tool also enables observation based on the observation plan and current aircraft traffic taking into account the type of object (custom, all, debris). The algorithm determines the list of objects based on the position of the station, the minimum angle of observation, including the observation of day/night observations. The next function of the program is the possibility to changing in semiRT timebias parameter of the pass, respect to predicted position of ephemeris and changing the position of the Az / El axis to improve data acquisition (mismatch of prediction). There is initial stage to correct the tracking trajectory of the object based on images of tracked object and its position into photo's frame using OpenCV in semiRT [7]. The software, parallel to the laser

range measurement, acquires angles based on the encoder data and information obtained from passive optical acquisition.

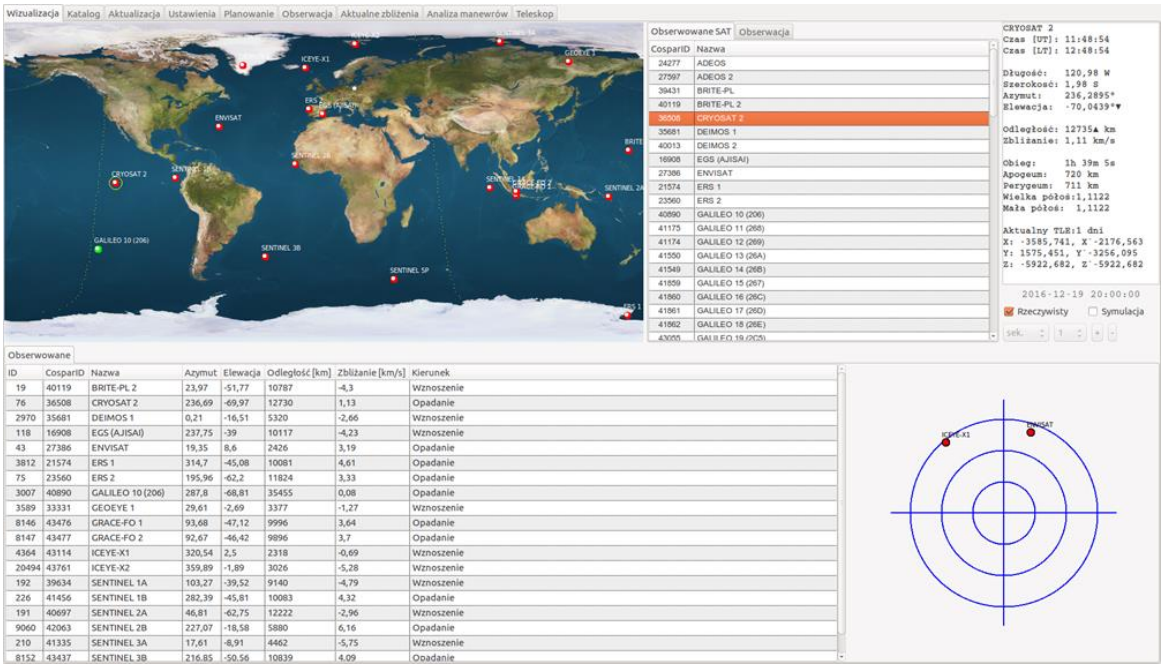

Fig. 4. Software tool for second setup control – global view window.

In order to carry out the positioning accuracy and tracking permanence test, satellites from the GEO to LEO regions to test campaign were selected. Objects from the LEO region were tracked in the day / night terminator. The first test concerned the positioning of the telescope and the quality of the images. To determine the accuracy of tracking, the 1 second exposure time of camera was selected (point - finite covering). The resultant field of view (FOV) of the tested telescope RC8" and the used camera ASI1600MMC was 38'x 29'. Tests were carried out on various nights due the overcast (Fig.5).

Fig. 5. Envisat (RC 8", ASI1600MMC, 1sec exposition).

4 TRACKED OBJECTS

The LASBOR sensor regularly tracks several dozen objects from LEO regime. This number is increasing systematically and currently is close to 100 objects. To the group of objects tracked by LASBOR sensor belong inactive/defunct satellites equipped with retroreflectors like ENVISAT, ERS-1, ERS-2, JASON-1, SEASAT-1, TOPEX / Poseidon and others as well as typical uncooperative boosters like ARIANE's, DELTA's, CZ's, SL's and TITAN's objects. Table 3 presents statistical results gathered by LASBOR station during the period 2016 - 2019. The Table 3 contains an information about number of all tracked objects during the giving years, number of

registered successful passes, number of normal points gained for all successful passes, number of single measurements collected for all successful passes and minimum / maximum values of RMS. The space debris laser used by LASBOR team has a pulse length 3 - 5 ns, which implies larger values of RMS. Some of rocket bodies were observed by means of picosecond laser module, i.e. objects NORAD's 28480 and 31114 (please see Table 4 below for more details).

Tab. 3. Observational statistics of the space debris for LASBOR station.

YEAR	TRACKED OBJECTS	REGISTERED PASSES	NORMAL POINTS	SINGLE MEASUREMENTS	RMS [cm]
2016	11	151	2 528	137 836	1.49-75.33
2017	12	251	3 529	230 901	5.18-81.60
2018	10	483	6 085	279 152	2.45-44.83
2019	38	389	4 074	189 024	2.04-221.72

All cooperative objects are observed from elevation 20 degrees, including illumination by the Sun and pass in Earth shadow. They are equipped with retroreflectors and allow to obtain the returns basically quickly and easily. All uncooperative objects are observed from elevation 30 degrees and close to the terminator. It is caused by a difficulty in tracking if the observed target is in Earth shadow. The input ephemeris is based on general TLE elements. This had an effect that an operator never knew, where the observed target could appear on the guiding monitor during the observations.

In Figures 6-9 the sample results of several observations of different rocket bodies are presented, i.e. SL, CZ-2C, ARIANE and TITAN. For better recognizability, in case of ARIANE and TITAN objects the good returns were marked by use of red ellipse.

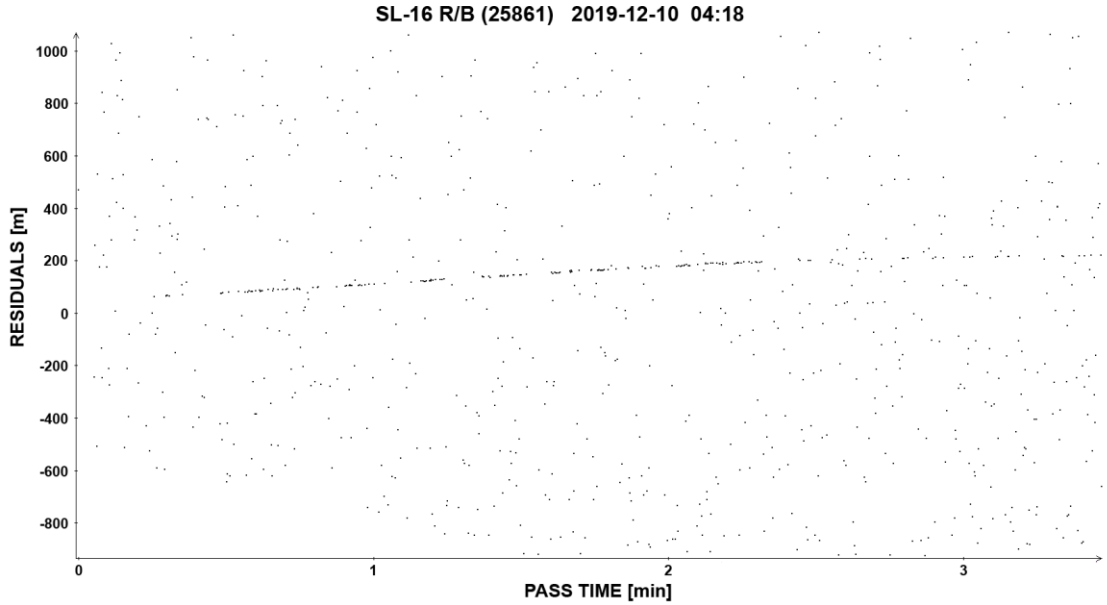

Fig. 6. The pass of SL rocket body with confirmed 169 returns.

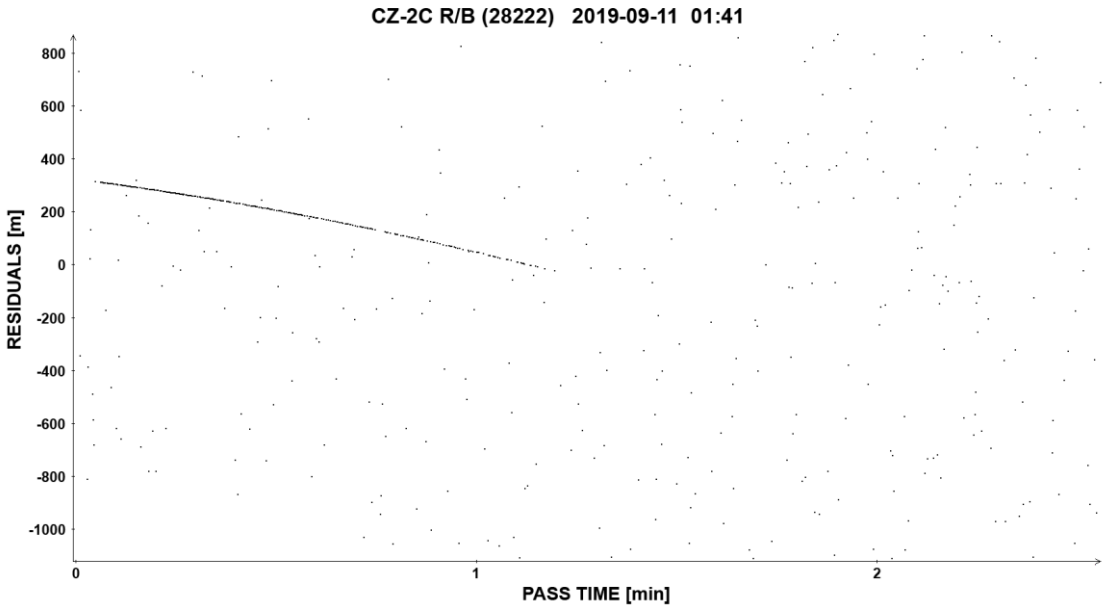

Fig. 7. The pass of CZ-2C rocket body with confirmed 276 returns.

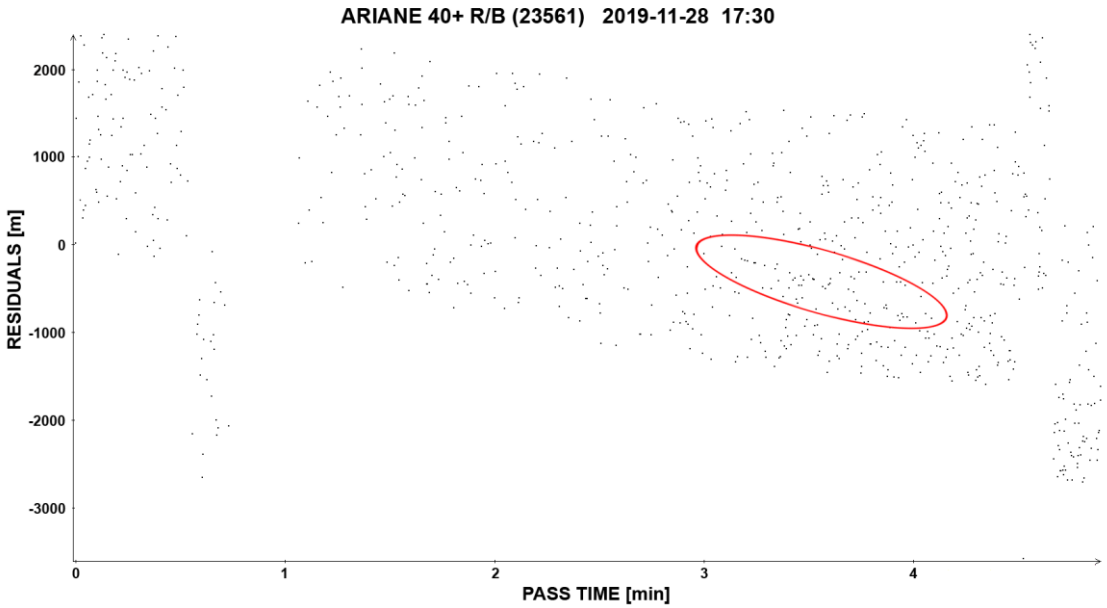

Fig. 8. The pass of ARIANE rocket body with confirmed 26 returns.

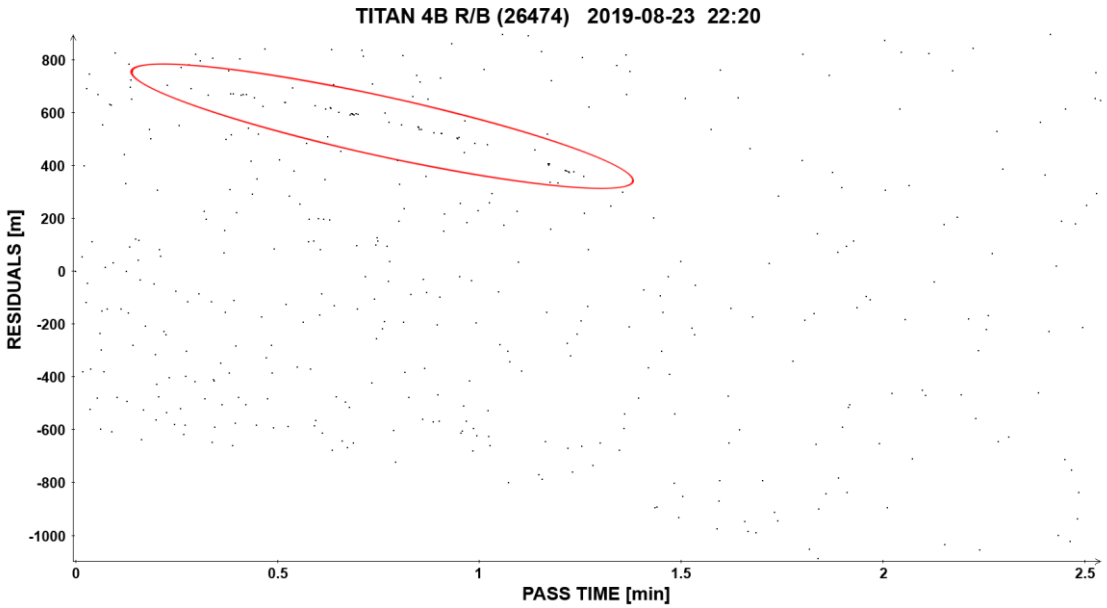

Fig. 9. The pass of TITAN rocket body with confirmed 48 returns.

5 ORBITAL CALCULATIONS

The LASBOR team specializes also in orbital calculations of satellites and space debris. For the needs of this study The orbits of 13 rocket bodies were calculated based on single measurements registered by the laser ranging sensor. In Table 4 all objects are listed with basic orbital parameters. Some of these objects are equipped with retroreflectors. This fact was confirmed by LASBOR station in case of to this work the advanced orbital programme were used GEODYN-II. All calculations were made in ECI TOD frame and including full force models and parameters according to the IERS Conventions. The input ephemeris was based on general TLE elements downloaded from the SPACETRACK database [12]. In Table 5 the results of orbital computations are presented, i.e. the number of the processed points (single measurements), the RMS of determined orbits, the RMS's of position and velocity. The number of processed points is from 19 to 276, the orbital RMS is from 3.40 cm to 2.2193 m. The value 3.40 cm concerns the object nr 10 in Tables 4 and 5 and results from the use of picosecond laser module (target is equipped with retroreflectors). With the retroreflectors is equipped also the object nr 9, what was confirmed by our team with picosecond laser module.

Tab. 4. Basic orbital parameters of the calculated rocket bodies.

NR	Object	NORAD	Perigee [km]	Apogee [km]	Incl. [^{0}]	Period [min]	RCS [m^2]
1	SL313121	13121	535.9	557.5	81.2	95.4	5.68
2	SL1420511	20511	625.2	647.5	82.5	97.3	4.78
3	SL820775	20775	374.2	1195.1	82.9	100.4	8.08
4	SL1622220	22220	836.6	852.4	71.0	101.7	15.16
5	SL1622803	22803	829.6	857.0	71.0	101.6	10.74
6	SL1625400	25400	806.2	822.0	98.6	101.0	12.03
7	TTN26474	26474	544.3	628.8	68.0	96.3	15.61
8	CZ2C28222	28222	509.9	574.6	97.7	95.3	12.4
9	CZ2C28480*	28480	711.2	915.2	98.1	101.0	10.56
10	CZ2C31114*	31114	791.1	878.5	98.3	101.5	8.26
11	CZ2C39203	39203	680.7	753.3	98.5	99.0	N/A
12	CZ4C39211	39211	471.3	643.5	98.0	95.7	N/A
13	CZ2C39364	39364	458.7	525.1	97.3	94.3	N/A

* Objects equipped with retroreflectors (confirmed independently by use of ps laser module)

Tab. 5. The results of the orbital computations.

NR	NORAD	POINTS	ORBITAL RMS [m]	RMS POS [m]	RMS VEL [m/s]
1	13121	36	0.9473	117.1480	1.1989
2	20511	27	2.2193	115.5452	1.0142
3	20775	61	0.5058	126.2387	1.1249
4	22220	33	0.8773	130.5872	0.9749
5	22803	21	1.9558	132.6775	1.1198
6	25400	47	0.9645	122.1392	0.9142
7	26474	19	0.4045	123.2564	1.2230
8	28222	276	0.2095	127.6070	1.1350
9	28480	186	0.4742	119.3398	1.1369
10	31114	87	0.0340	132.3284	1.1136
11	39203	38	1.0233	127.0835	1.0309
12	39211	30	0.6092	91.4257	1.0845
13	39364	54	0.4775	117.9716	1.2682

The RMS POS and RMS VEL were calculated according to the following formulas:

$$RMS\ POS = \sqrt{(S_X + S_Y + S_Z)} \tag{1}$$

where S_X, S_Y, S_Z are standard deviations of position components X, Y and Z, respectively.

$$RMS\ VEL = \sqrt{(S_{Vx} + S_{Vy} + S_{Vz})} \tag{2}$$

where S_{Vx}, S_{Vy}, S_{Vz} are standard deviations of velocity components V_X, V_Y and V_Z, respectively.

The second step of the orbital computations was to determine the cartesian variance-covariance (VARCOV) matrices for all calculated objects. The reference cartesian VARCOV matrix was defined as presented in Table 6, i.e. 100 m for position components and 1.0 m/s for velocity components. The units of input VARCOV elements are m^2, m^2/s and m^2/s^2, respectively. The calculated VARCOV matrices of all objects are presented in Tables 7 - 19. Based on the obtained results the output VARCOV matrices were improved by approximately 20 - 40%. These results show how big contribution to the improvement of the orbital information about the tracked objects can gives one short single laser track. The length of the input full rate data files was from 45 till 173 seconds. For each object only one track was processed.

Tab.6. The input VARCOV matrix.

Input VARCOV elements	X	Y	Z	Vx	Vy	Vz
X	10000.0	10000.0	10000.0	100.0	100.0	100.0
Y	10000.0	10000.0	10000.0	100.0	100.0	100.0
Z	10000.0	10000.0	10000.0	100.0	100.0	100.0
Vx	100.0	100.0	100.0	1.0	1.0	1.0
Vy	100.0	100.0	100.0	1.0	1.0	1.0
Vz	100.0	100.0	100.0	1.0	1.0	1.0

Tab.7. The calculated VARCOV matrix for object 13121.

13121	X	Y	Z	Vx	Vy	Vz
X	7878.3804	3362.5730	626.5734	-0.4825	-12.2482	15.9740
Y	3362.5730	3041.8069	2370.4176	-0.9945	12.7548	-13.4983
Z	626.5734	2370.4176	2803.4714	-0.8722	22.7194	-25.2698
Vx	-0.4825	-0.9945	-0.8722	0.6314	0.3814	0.1940
Vy	-12.2482	12.7548	22.7194	0.3814	0.4623	-0.1382
Vz	15.9740	-13.4983	-25.2698	0.1940	-0.1382	0.3436

Tab.8. The calculated VARCOV matrix for object 20511.

20511	X	Y	Z	Vx	Vy	Vz
X	6549.7806	4014.3747	-2167.1376	-9.6474	-0.7299	-3.1492
Y	4014.3747	2495.4091	-976.6037	-9.1502	-0.1626	-2.9850
Z	-2167.1376	-976.6037	4305.4983	-32.1392	1.9225	-8.5757
Vx	-9.6474	-9.1502	-32.1392	0.7696	0.2132	-0.1049
Vy	-0.7299	-0.1626	1.9225	0.2132	0.1293	-0.1187
Vz	-3.1492	-2.9850	-8.5757	-0.1049	-0.1187	0.1297

Tab.9. The calculated VARCOV matrix for object 20775.

20775	X	Y	Z	Vx	Vy	Vz
X	9134.8248	1566.9986	1919.3626	0.0755	5.3999	-9.3623
Y	1566.9986	6038.0049	-1111.4140	-0.0134	-18.8404	31.2444
Z	1919.3626	-1111.4140	763.3684	0.0519	6.0726	-10.1727
Vx	0.0755	-0.0134	0.0519	0.8697	0.3013	0.1427
Vy	5.3999	-18.8404	6.0726	0.3013	0.1755	-0.0684
Vz	-9.3623	31.2444	-10.1727	0.1427	-0.0684	0.2203

Tab.10. The calculated VARCOV matrix for object 22220.

22220	X	Y	Z	Vx	Vy	Vz
X	4541.0728	-3296.0787	3437.5891	9.8199	0.3748	-9.2232
Y	-3296.0787	7586.5471	977.9155	15.3246	-2.6234	-17.4248
Z	3437.5891	977.9155	4925.3934	22.6592	-1.4979	-23.0204
Vx	9.8199	15.3246	22.6592	0.4122	-0.3275	0.0098
Vy	0.3748	-2.6234	-1.4979	-0.3275	0.3463	-0.1351
Vz	-9.2232	-17.4248	-23.0204	0.0098	-0.1351	0.1919

Tab.11. The calculated VARCOV matrix for object 22803.

22803	X	Y	Z	Vx	Vy	Vz
X	6975.9364	1362.8640	1825.4796	13.8691	-16.5295	-33.4453
Y	1362.8640	8244.8860	-3541.4148	-2.4862	0.6378	0.5638
Z	1825.4796	-3541.4148	2382.4951	6.2184	-6.2423	-12.2141
Vx	13.8691	-2.4862	6.2184	0.0695	0.0960	-0.1277
Vy	-16.5295	0.6378	-6.2423	0.0960	0.8683	-0.2690
Vz	-33.4453	0.5638	-12.2141	-0.1277	-0.2690	0.3163

Tab.12. The calculated VARCOV matrix for object 25400.

25400	X	Y	Z	Vx	Vy	Vz
X	7418.4337	2386.5991	1982.8584	9.3269	20.2535	-13.2975
Y	2386.5991	6968.2283	716.2551	-11.1095	-26.5209	14.3247
Z	1982.8584	716.2551	531.3144	2.4762	5.1260	-3.2840
Vx	9.3269	-11.1095	2.4762	0.3229	0.3282	0.0082
Vy	20.2535	-26.5209	5.1260	0.3282	0.4170	-0.0805
Vz	-13.2975	14.3247	-3.2840	0.0082	-0.0805	0.0959

Tab.13. The calculated VARCOV matrix for object 26474.

26474	X	Y	Z	Vx	Vy	Vz
X	6093.6551	-871.0202	3345.9729	6.1173	30.7353	-14.1682
Y	-871.0202	2642.6589	2931.5875	-4.1332	-29.0782	12.0565
Z	3345.9729	2931.5875	6455.8263	-0.9691	-16.5648	5.7589
Vx	6.1173	-4.1332	-0.9691	0.3943	0.1988	0.4289
Vy	30.7353	-29.0782	-16.5648	0.1988	0.4504	0.0052
Vz	-14.1682	12.0565	5.7589	0.4289	0.0052	0.6510

Tab.14. The calculated VARCOV matrix for object 28222.

28222	X	Y	Z	Vx	Vy	Vz
X	6708.8545	787.1819	3552.8935	3.8427	-25.5435	-13.5556
Y	787.1819	4596.1175	-3317.8276	2.3977	-32.3603	-14.6036
Z	3552.8935	-3317.8276	4978.5746	0.4524	10.8092	3.6396
Vx	3.8427	2.3977	0.4524	0.4192	-0.2243	0.4051
Vy	-25.5435	-32.3603	10.8092	-0.2243	0.3823	-0.0622
Vz	-13.5556	-14.6036	3.6396	0.4051	-0.0622	0.4866

Tab.15. The calculated VARCOV matrix for object 28480.

28480	X	Y	Z	Vx	Vy	Vz
X	6131.0274	4542.7530	-478.5494	4.8384	-5.8813	9.4369
Y	4542.7530	4479.7076	1646.0555	-3.2226	3.9689	-6.7616
Z	-478.5494	1646.0555	3631.2504	-12.6338	15.3992	-25.4462
Vx	4.8384	-3.2226	-12.6338	0.6091	0.4304	0.1736
Vy	-5.8813	3.9689	15.3992	0.4304	0.4871	-0.0411
Vz	9.4369	-6.7616	-25.4462	0.1736	-0.0411	0.1963

Tab.16. The calculated VARCOV matrix for object 31114.

31114	X	Y	Z	Vx	Vy	Vz
X	1230.5145	1815.3238	-2701.6875	-4.1464	0.7686	-1.3026
Y	1815.3238	8468.9841	-687.3847	27.0219	-1.0463	13.4381
Z	-2701.6875	-687.3847	7811.3106	27.9320	-3.0344	11.6381
Vx	-4.1464	27.0219	27.9320	0.3182	0.2267	-0.1118
Vy	0.7686	-1.0463	-3.0344	0.2267	0.5117	-0.4364
Vz	-1.3026	13.4381	11.6381	-0.1118	-0.4364	0.4102

Tab.17. The calculated VARCOV matrix for object 39203.

39203	X	Y	Z	Vx	Vy	Vz
X	8899.7311	-1340.4609	1146.2071	-7.5496	16.3754	15.5872
Y	-1340.4609	2748.4381	-3502.3712	-5.4166	17.0253	13.4895
Z	1146.2071	-3502.3712	4502.0537	7.7997	-23.4898	-18.5978
Vx	-7.5496	-5.4166	7.7997	0.5185	-0.2981	0.1975
Vy	16.3754	17.0253	-23.4898	-0.2981	0.2907	0.0310
Vz	15.5872	13.4895	-18.5978	0.1975	0.0310	0.2536

Tab.18. The calculated VARCOV matrix for object 39211.

39211	X	Y	Z	Vx	Vy	Vz
X	6615.9072	3379.8947	-2.8647	-5.4788	16.1247	-28.1187
Y	3379.8947	1741.7466	1.9719	-2.7846	8.2072	-14.5095
Z	-2.8647	1.9719	0.9974	-0.0063	0.0192	-0.0309
Vx	-5.4788	-2.7846	-0.0063	0.9692	0.1423	-0.0717
Vy	16.1247	8.2072	0.0192	0.1423	0.0761	-0.0862
Vz	-28.1187	-14.5095	-0.0309	-0.0717	-0.0862	0.1310

Tab.19. The calculated VARCOV matrix for object 39364.

39364	X	Y	Z	Vx	Vy	Vz
X	6905.7087	2572.8571	1977.1268	5.3397	-18.3310	26.5067
Y	2572.8571	6103.2164	2063.4400	-6.6181	20.5890	-28.3133
Z	1977.1268	2063.4400	908.3814	-0.7018	1.8477	-2.2684
Vx	5.3397	-6.6181	-0.7018	0.5221	0.3887	0.2969
Vy	-18.3310	20.5890	1.8477	0.3887	0.6113	-0.0853
Vz	26.5067	-28.3133	-2.2684	0.2969	-0.0853	0.4751

Additionally, the computed (corrected) positions of the objects were transformed to the RSW frame and compared with the input ephemeris. The results of this comparison are presented in Figure 10. In Table 20 the differences

for all RSW components are shown, which as the absolute numbers are from 20 m to 258 m for radial component, from 22 m to 685 m for along - track component and from 6 to 595 m for cross - track component, respectively.

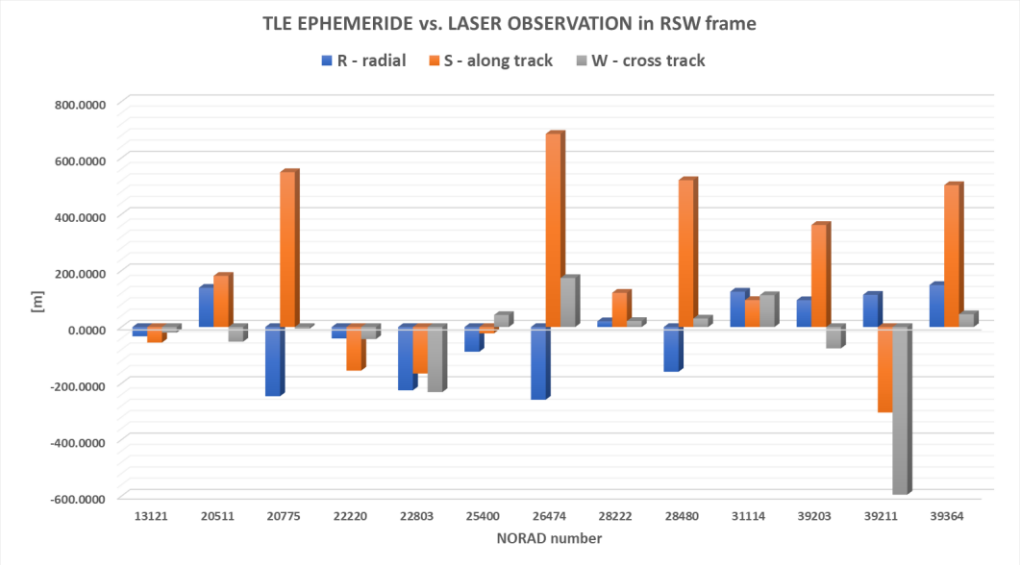

Fig. 10. Comparison an input ephemeris with new positions computed based on laser measurements.

Tab.20. The differences in RSW frame between input ephemeris and computed (corrected positions).

NR	NORAD	R [m]	S [m]	W [m]
1	13121	-32.7300	-55.1021	-19.7875
2	20511	139.2259	181.5438	-51.8603
3	20775	-245.5797	549.5603	-5.9242
4	22220	-40.5938	-154.6200	-42.8011
5	22803	-224.5271	-164.8346	-230.7056
6	25400	-87.7135	-22.2680	42.6446
7	26474	-257.9778	685.3597	173.8262
8	28222	20.3679	121.3771	21.2288
9	28480	-158.6727	521.1973	30.1375
10	31114	125.3883	95.5015	113.0499
11	39203	95.2095	361.9902	-75.8052
12	39211	114.3450	-303.1528	-594.8407
13	39364	149.0449	503.4823	45.3641

6 SUMMARY & OUTLOOK

The laser tracking of space debris objects (uncooperative objects especially) is very challenging and from laser sensors requires regularity and cooperation of many factors such as: continuous and sustained work of the sensor composed from many different elements (i.e. the integrated work of all components), an initial information about current location of the tracked object (the accuracy of the initial orbital information), weather conditions (how is the weather during the observations), safety aspects (permanent monitoring of sky because of air traffic), a man's contribution (a human can always miss something). The primary conclusion to laser tracking is, that the tracking of invisible objects basing on general TLE elements is very hard and ineffective, because they have inaccurate ephemerides, and the system does not know where the objects is on the sky during the observation (there is no returns; time loss). Therefore, for a night-tracking we recommend the tracking close to the terminator. The secondary conclusion to the laser tracking is, that the same object should be tracked by more than one station to improve the accuracy of its TLE's elements. However, based on the presented orbital calculations of several objects we see clearly, that even very short single laser track (order of several dozen of seconds) improves their VARCOV's information about 20 - 40%.

In the context of space debris monitoring, catalogue building, space debris nudging, conducting for space debris mitigation, the future belongs to the laser technology (more powerful lasers, more effective detection systems,

laser tracking of smaller objects, increasing the range of the laser tracking, laser day tracking etc.). All aspects mentioned above will strengthen the global Space Situational Awareness (SSA), significantly.

7 REFERENCES

[1] B. Greene, Y. Gao, C. Moore, Y. Wang, A. Boiko, J. Ritchie, J. Sang, J. Cotter. *Laser tracking of space debris*, Proceedings of 13th Laser Ranging Workshop, Washington, 2002.

[2] G. Kirchner, F. Koidl, F. Friederich, I. Buske, U. Volker, W. Riede. *Laser measurements to space debris from Graz SLR station*, Advances in Space Research, Vol. 51, Issue 1, pp. 21-24, 2012.

[3] Zhang, Z.P., Yang, F.M., Zhang, H.F., Wu, Z.B., Chen, J.P., Li, P., Meng, W.D. *The use of laser ranging to measure space debris*, Res. Astron. Astrophys. 12 (2), 2012.

[4] C. R. Phipps and C. Bonnal. *A spaceborne, pulsed UV laser system for re-entering or nudging LEO debris, and re-orbiting GEO debris*. Acta Astronaut. 118, 224–236, 2016.

[5] Z. Zhongping, D. Huarong, T. Kai, W. Zhibo, Z. Haifeng. *Development of Laser Measurement to Space Debris at Shanghai SLR Station*, Proceedings of the 7th European Space Debris Conference, Paper No. 255, ESA/ESOC, Darmstadt, April 18-21, 2017.

[6] Z. Liang, X. Dong, M. Ibrahim, Q. Song, H. Xingwei, C. Liu, H. Zhang, G. Zhao, *Tracking the space debris from the Changchun Observatory*, Astrophysics and Space Science 364. doi:10.1007/s10509-019-3686-x, 2019.

[7] M. Steindorfer, G. Kirchner, F. Koidl, P. Wang, B. Jilete, T. Flohrer, *Daylight space debris laser ranging, Nature Communications*, 11, Article number: 3735, doi:10.1038/s41467-020-17332-z, 2020.

[8] ILRS NETWORK, Borowiec laser station, *https://ilrs.gsfc.nasa.gov/network/stations/active/BORL_general.html*, 2020.

[9] P. Lejba, T. Suchodolski, P. Michałek, J. Bartoszak, S. Schillak, S. Zapaśnik. *First laser measurements to space debris in Poland*, Advances in Space Research, Vol. 61, Issue 10, pp. 2609–2616, DOI: https://doi.org/10.1016/j.asr.2018.02.033, 2018.

[10] B. Jilete, T. Flohler, A. Mancas, J. Castro, J. Siminski. *Acquiring observations for test and validation in the space surveillance and tracking segment of esa's ssa programme*, Journal of Space Safety Engineering. 6 (2019) 197 – 200, doi:10.1016/j.jsse.2019.05.003, 2019.

[11] D.E. Pavlis, S. Luo, P. Dahiroc et al. *GEODYN II System Description*, Hughes STXContractor Report, Greenbelt, Maryland, 1998.

[12] SPACETRACK service, *https://www.space-track.org/*, 2020.